



The effect of carrier in KCoMoS-supported catalysts for hydro-upgrading of model FCC gasoline

D. Ishutenko^a, Yu. Anashkin^a, P. Nikulshin^{a,b,*}

^a Samara State Technical University, 244 Molodogvardiyskaya st., Samara, 443100, Russia

^b All-Russia Research Institute of Oil Refining, 6 Aviamotornaya st., Moscow, 111116, Russia



ARTICLE INFO

Keywords:

Selective hydrodesulfurization
Selective hydrogenation
KCoMoS
FCC gasoline
Diolefin

ABSTRACT

K-CoMo/Sup (where Sup = Al₂O₃, SiO₂, TiO₂ and ZrO₂) catalysts were synthesized using H₃PMo₁₂O₄₀, CoCO₃, KOH and citric acid. The catalysts were characterized by temperature-programmed reduction (TPR), temperature-programmed desorption of NH₃, X-ray photoelectron spectroscopy, transmission electron microscopy. Samples were tested in hydrotreating of model fluid catalytic cracking gasoline and in selective hydrogenation of 1,5-hexadiene and *n*-heptene-1. The type of used carrier significantly affected the morphology of active phase and catalytic properties. Active sites productivity of K-CoMo/Sup catalysts in hydrodesulfurization (HDS) and olefin hydrogenation (HYDO) reactions as well as HDS/HYDO selectivity correlated with active phase morphology excepting TiO₂-supported sample. Productivity of active sites in reactions of selective hydrogenation of diolefin depended on maximum peak reduction obtained from TPR, which in turn was a function of acidity of using supports. The highest HDS/HYDO selectivity was obtained at catalyst which possessed the lowest selectivity towards partial hydrogenation of diolefine compared to complete hydrogenation.

1. Introduction

The consumption of motor fuels in the world is increasing every year [1]. At the same time, the ecological and on-the-road requirements to commercial fuels are becoming tougher because of continuous deterioration of oil quality. In the meantime, the production of oil fractions of a secondary origin, with the specific chemical composition, requiring the qualified processing is increasing due to the necessity of raising the oil conversion ratio. At the same time, it increases annual production of FCC gasoline – a high-octane component of the commercial fuel that is characterized by considerable content of sulfur (up to 1.5% wt. depending on the using of hydrotreating of vacuum gasoil before FCC processing) and large number of olefins [2]. Therefore, in order to meet the modern ecological requirements, it is necessary to upgrade the FCC gasoline before its compounding. Conventional Co(Ni) Mo/Al₂O₃ catalysts are not suitable for the current process, since they lead to considerable decrease of research octane number (RON) due to hydrogenation of olefins. As a result, in addition to hydrotreating the hydrotreated product should pass through octane-recovering processes. Development of highly selective towards sulfur removal reactions catalysts which will allow carrying out the process of hydrotreating of FCC gasoline with preservation of octane number is much more preferable because it demands lower operational costs and can be carried out at

the facilities which are available at oil refineries. In that context supported K-modified transition metal sulfides (TMS) are promising due to their low olefin hydrogenation (HYDO) and reasonable hydrodesulfurization (HDS) activities [3–8].

Aside from the problem of reducing sulfur with RON maintenance, the issue of decreasing of diolefin amount is also of key importance. Diolefins should be hydrogenated before desulfurization to avoid gum formation due to diolefin polymerization [9], to prevent HDS catalyst deactivation and to minimize the possible recombination of H₂S and diolefins with formation of mercaptans [2]. In commercial process there is a selective hydrogenation unit before hydrotreating one for transformation of diolefins into olefins [10]. Though the process has been implemented in the industry there is some open data related to catalysts, used in selective hydrogenation of diolefins from FCC gasoline. Typically supported Pt- or Pd-based [11–15] and Ni-based [16–19] catalysts are used for selective hydrogenation of diolefins in pyrolysis gasoline with low amount of sulfur. In that context it will be beneficial to find the catalytic system appropriate for both selective hydrogenation of diolefins and selective HDS of FCC gasoline. It is well-known that the nature of the support plays one of the key roles in formation of active phase of TMS catalysts [20–24]. The type of the carrier impacts the dispersion, morphology and electronic properties of the active phase species, besides the type of hydrotreating feed defines the

* Corresponding author at: Samara State Technical University, 244 Molodogvardiyskaya st., Samara, 443100, Russia.

E-mail address: p.a.nikulshin@gmail.com (P. Nikulshin).

textural characteristics of applying catalyst [25]. There are three main approaches to choosing the catalyst support: using hierarchical mesoporous alumina [26–28], modifying alumina with metals, oxides and so on [29–37], applying alternative carriers such as SiO_2 , TiO_2 , ZrO_2 and others [38–42].

Li and co-workers [43] determined the relation between active phase morphology and HDS/HYDO selectivity of CoMo catalysts supported on alumina and silica. Furthermore, the authors discovered that the active phase properties are related to the type of used carrier. Thus, the longest average slab length and the highest edge/corner ratio and the best HDS/HYDO selectivity were obtained on CoMo/ SiO_2 catalyst.

Mochizuki et al. studied the relation between acidic properties of CoMo catalysts and their catalytic properties [44]. They have found that selectivity of SiO_2 -supported catalyst is higher than that of Al_2O_3 -supported one. CoMo/ Al_2O_3 catalyst possessed more coordinatively unsaturated sites, so-called CUS-sites, than CoMo/ SiO_2 sample, though the reactivity of these sites was lower. As the result, the authors concluded that controlling of the amount of Lewis acid sites of the carrier and sulfided active phase particles allows to achieve better HDS/HYDO selectivity.

Basically SiO_2 -supported catalysts reported as most HDS/HYDO selective, connected mostly to low acidity and reduced interacting of the carrier and active phase species. At the same time, the HDS activity of such catalysts is not as high as desired due to the low dispersion of crystallites of CoMoS active phase. On the other hand, Al_2O_3 -supported catalysts are mostly more active but as HDS/HYDO selective as SiO_2 -supported ones. Reducing the acidity of alumina with different additives improves HDS/HYDO selectivity.

Perez-Martinez et al. [45] evaluated the CoMo catalysts, supported on amorphous aluminosilicates (ASA) with different Si/(Si + Al) ratios in hydrotreating of model FCC gasoline. They established that increasing of Si/(Si + Al) ratio favored inhibition of both HDS and HYDO reactions. At the same time acid-type reactions like alkylation of S-containing compound with olefins, isomerization and cracking of olefins were presented. These changes were explained by the growth of strength of Brønsted sites. In further investigation [46] the authors concluded that highly selective hydrotreating catalyst should possessed only weak Brønsted acidity because such active centers favor the migration of double bond from terminal position deeply into the molecule.

Nadeina and co-workers [47] investigated the influence of Mg as the additive to CoMo/ Al_2O_3 -ASA catalyst for selective hydrotreating of FCC gasoline. They studied different ways of Mg introduction into the catalyst, among which were addition of it to ASA and to kneading paste during the support preparation as well. Testing the synthesized catalytic systems in hydrotreating of model FCC gasoline showed the positive impact of Mg on HDS activity value. However, the influence on HYDO and isomerization reactions was different depending on the ways of Mg introduction. In the case of adding Mg into ASA, the authors observed a slight effect on catalyst activity that was connected to decreasing of active phase dispersion due to lowering of surface area and pore volume compared to CoMo/ Al_2O_3 -ASA sample. Meanwhile, in the case of introducing Mg into kneading paste, the value of HYDO activity was lower due to good-balanced set of Lewis and Brønsted acid sites and changing the active phase morphology.

Klimova et al. [48] investigated the impact of the amount of magnesia in alumina-magnesia supports on activity in HDS and HYDO reactions for Mo and NiMo catalysts. It was revealed that incorporation of even small amounts of magnesia led to a significant decrease of HYDO activity whereas HDS activity did not drop much. The authors connected the observed phenomena with formation of magnesium molybdate and solid solution of NiO and MgO. Moreover, using magnesia in the support provided the MoS_2 slab length extension.

Muralidhar et al. [49] reported the impact of the support of CoMo catalysts on the HDS of thiophene and hydrogenation of *n*-hexene-1. They obtained that catalysts synthesized on the base of different types of Al_2O_3 were more effective in both types of the reactions than the

samples supported on SiO_2 - Al_2O_3 , SiO_2 -MgO and TiO_2 . It was attributed to a high dispersion of the active phase species on the surface of Al_2O_3 . For SiO_2 -containing catalysts the decrease of HDS and HYDO activity with simultaneous increase of HDS/HYDO selectivity was observed.

In our previous works the effect of modification of the active phase species by potassium [7,8] was studied. Simultaneous introduction of alkali metal with $\text{H}_3\text{PMo}_{12}\text{O}_{40}$ and cobalt citrate significantly favored the HDS/HYDO selectivity with reasonable decrease of HDS activity that makes trimetallic KCoMoS catalysts promising for selective hydrotreating of FCC gasoline. Addition of phosphorus to hydrotreating catalyst favored the dispersion of active phase species and selective formation of CoMoS active phase [50–53] whereas using of alkali metal led to partial poisoning of active sites with the reduction of activity [3,4] as the result simultaneous use of potassium and phosphorus allowed to achieve synergism and good-balance between activity and HDS/HYDO selectivity [5,6]. However, there is no systematical research of the impact of the carrier nature on the properties of trimetallic supported catalyst. The current study is focused on the influence of the type of the support used in preparation on physical-chemical characteristics of KCoMoS active phase and its action in selective HDS of model FCC gasoline as well as selective diolefin hydrogenation.

2. Experimental

2.1. Catalyst preparation

K-Co-PMo/Sup catalysts were prepared by means of wetness impregnation technique of the different carriers (Al_2O_3 , SiO_2 , TiO_2 and ZrO_2) with joint aqueous solutions of active components in the required quantities. From the point of phase composition of the carriers silica was used in amorphous state (Sigma-Aldrich), TiO_2 was used as anatase (ChemPur), ZrO_2 (ChemPur) was a mixture of monoclinic and tetragonal phases and alumina (Sasol) was used in γ -phase. $\text{H}_3\text{PMo}_{12}\text{O}_{40}$, cobalt citrate and potassium hydroxide were used as precursors. For all the catalysts, the atomic ratios of Co/Mo and K/Mo were maintained at the levels of 0.5 and 2.0, respectively. To mitigate the impact of specific surface area of used carrier on the dispersion of active phase species the surface concentration of Mo was fixed at the value of 4 at Mo/nm^2 . The catalysts preparation protocol was followed. Firstly, the solution of cobalt citrate was prepared by dissolving CoCO_3 and citric acid. Next, the solution of $\text{H}_3\text{PMo}_{12}\text{O}_{40}$ in hot water was prepared. As the third step, the two solutions were mixed and cooled down, followed by adding the KOH. Finally, the dried supports were impregnated with prepared solutions and aged at room temperature during the night. All the samples were air-dried at 110 °C for 5 h. An EDX800HS analyzer was used to determine the exact content of loaded metals. For physical-chemical analysis, the synthesized catalysts were activated by sulfidation procedure in a flow of H_2S (15 vol. %) in H_2 at 400 °C for 2 h. The chemical composition and textural characteristics of synthesized K-Co-PMo/Sup catalysts are listed in Table 1.

2.2. Catalysts characterisation

To define the differences between using carriers, the acidity of the support materials was measured by temperature-programmed NH_3 desorption technique. The analyses were conducted at TPDRO 1100 analyzer. Firstly, samples were outgassed in helium flow at 550 °C during 1 h. NH_3 adsorption was conducted at 60 °C in the flow of NH_3/N_2 (1:1), purified by granulated NaOH. Full saturation of supports with ammonia was achieved after 30 min. Following that procedure weakly bonded NH_3 was removed by heating of samples in a helium flow at 100 °C during 1 h. Then the reactor was cooled down to room temperature. The NH_3 -TPD analysis was conducted in helium flow with the rate of 30 ml/min in the temperature range of 25 and 750 °C and heating rate of 8 °C/min.

Textural properties of support materials and catalysts were obtained

Table 1

Chemical composition and textural characteristics of synthesized K-Co-PMo/Sup catalysts.

Catalyst	Acidity of support ($\mu\text{mol NH}_3\text{ g}^{-1}$)	Content (wt. %)	Textural characteristics of sulfided catalyst										
						SSA ^a ($\text{m}^2\text{ g}^{-1}$)	PV ^b ($\text{cm}^3\text{ g}^{-1}$)	ED ^c (nm)	Pore size distribution (vol. %)				
			Co	Mo	K				< 2 nm	2-4 nm	4-20 nm	20-50 nm	> 50 nm
K-Co-PMo/SiO ₂	53		4.2	13.7	11.2	104	0.33	8.9	0	2	95	1	2
K-Co-PMo/TiO ₂	285		2.3	7.6	6.2	70	0.24	3.8/9.5	0	9	59	20	12
K-Co-PMo/ZrO ₂	113		1.8	6.0	4.9	50	0.17	3.8/6.8/11.6	0	8	72	15	5
K-Co-PMo/Al ₂ O ₃	200		2.9	9.3	7.6	119	0.31	7.2/10.2	0	4	94	1	1

^a Specific surface area.^b Pore volume.^c Effective diameter.

with applying low-temperature nitrogen adsorption performed on Quantachrome Autosorb-1 adsorption porosimeter. The specific surface area was calculated in accordance with BET methodology at relative partial pressures (P/P_0) ranging from 0.05 to 0.3. The total pore volume and pore size distribution were estimated from the desorption curve using BJH model at a P/P_0 of 0.99.

Morphological characteristics of KCoMoS active phase species were calculated from data obtained by high resolution transition electronic microscopy for sulfided K-Co-PMo/Sup catalysts. HRTEM micrographs were recorded by Tecnai G2 20 electron microscope and analyzed by the Fourier method. The average slab length (\bar{L}) and stacking number (\bar{N}) were defined for each sample statistically by handling more than 400 slabs. The average slab length \bar{L} was calculated as an average number of manually defined linear sizes of slabs and the stacking number was determined as a number of slabs per stack:

$$\bar{N} = \frac{\sum_{i=1..t} n_i N_i}{\sum_{i=1..t} n} \quad (1)$$

Where, n_i is the number of stacks with N_i layers.

MoS₂ slabs were assumed as perfect hexagons [54] for simplifying the calculation of geometrical characteristics of active phase species. Thus, for all catalysts the edge-to-corner ratio of a MoS₂ slab (f_e/f_c)_{Mo} was calculated as following [43]:

$$(f_e/f_c)_{\text{Mo}} = \frac{Mo_e}{Mo_c} = \frac{10 \times \bar{L}/3.2 - 3}{2} \quad (2)$$

Where, Mo_e is the total number of Mo atoms at the edge surface, Mo_c is the number of corner Mo atoms, \bar{L} is the average slab length.

X-ray photoelectron spectroscopy (XPS) spectra of sulfided catalysts were obtained by Kratos Axis Ultra DLD spectrometer with a monochromatic AlK_a source ($h\nu = 1486.6\text{ eV}$, 150 W). The binding energy (BE) values were calibrated by the positions of Au 4f_{7/2} (83.96 eV) and Cu 2p_{3/2} (932.62 eV) peaks. The spectral regions of Al 2p, S 2p, S 2s, Mo 3d, C 1s, K 2p, O 1s, Co 2p were recorded for each sample. The collected spectra were handled by a mixed Gaussian (30%) – Lorentzian (70%) method with the use of CasaXPS software program. A Shirley background subtraction was applied for atomic concentrations calculation. The decompositions of the S 2p, Mo 3d and Co 2p XPS spectra were performed using the appropriate oxide and sulfided references as supported monometallic catalysts [7,55,56]. The decomposition of recorded spectra allowed calculating the relative amount of each active phase species in sulfided K-Co-PMo/Sup catalysts with the following equation:

$$[\text{CoMoS}] (\%) = \frac{A_{\text{CoMoS}}}{A_{\text{CoMoS}} + A_{\text{CoS}_x} + A_{\text{Co}^{2+}}} \times 100 \quad (3)$$

Where, A_x represented the peak area of species x.

To estimate the promotion ratio of MoS₂ slab edges the following equation was used:

$$(\text{Co/Mo})_{\text{edge}} = \frac{(\text{Co/Mo})_{\text{slab}}}{Mo_e + Mo_c} \times Mo_T = \frac{(\text{Co/Mo})_{\text{slab}}}{D} \quad (4)$$

Where, D is the dispersion of the active phase species calculated from TEM results and $(\text{Co/Mo})_{\text{slab}}$ is the promotion ratio of MoS₂ slabs, which was calculated as follows:

$$D = \frac{Mo_e + Mo_c}{Mo_T} = \frac{\sum_{i=1..t} 6n_i - 6}{\sum_{i=1..t} 3n_i^2 - 3n_i + 1} \text{ and } (\text{Co/Mo})_{\text{slab}} = \frac{C_{\text{CoMoS}}}{C_{\text{MoS}_2}} \quad (5)$$

where Mo_e is the total number of Mo atoms at the edge surface, Mo_c is the number of corner Mo atoms, Mo_T is the total number of Mo atoms, n_i is the number of Mo atoms along one side of the MoS₂ slab, as determined by its length, and t is the total number of slabs in the TEM micrograph; C_{CoMoS} and C_{MoS_2} is the absolute concentration of Co and Mo in the CoMoS and MoS₂ species respectively (at. %).

The effective Co content in CoMoS active phase was calculated as follows:

$$C_{\text{CoMoS}} = [\text{CoMoS}] \times C(\text{Co})_T \quad (6)$$

Where, $C(\text{Co})_T$ was referred to the effective concentration of cobalt determined by XPS (wt. %).

From the XPS and HRTEM results the edge-to-corner ratio of the CoMoS₂ slabs was calculated as following:

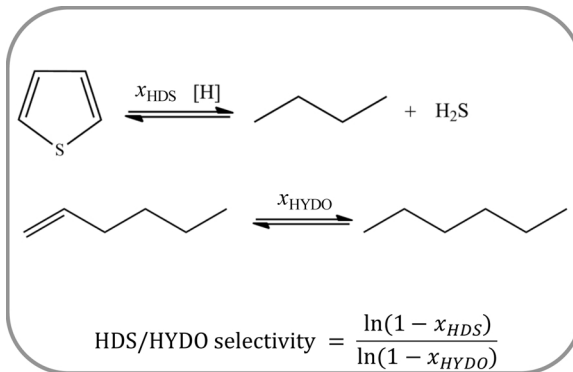
$$(f_e/f_c)_{\text{CoMo}} = (f_e/f_c)_{\text{Mo}} \times (\text{Co/Mo})_{\text{edge}} \quad (7)$$

The temperature-programmed reduction (TPR) of sulfided catalysts was conducted to evaluate the strength of Mo-S bonds. The catalyst samples (~0.25 g) were activated by gas-phase sulfidation process with a mixture of 10 vol. % of H₂S in H₂ at 400 °C during 4 h. The catalyst reduction was performed in a flow of 5 vol. % of H₂ in N₂. TPR profiles were recorded with the use of thermal conductivity detector (TCD) under the following conditions: temperature range from room to 900 °C, holding period at 900 °C of 1 h, heating rate of 10°/min, volume flow rate of 25 ml/min.

2.3. Catalytic properties evaluation

Catalytic activity and selectivity of synthesized samples was evaluated in two different processes and feed: hydrotreating and selective hydrogenation.

For studying the catalyst performance in hydrotreating the following model mixture was used: 1000 ppm of sulfur from thiophene, 36 wt. % of n-hexene-1, n-heptane as a solvent and n-octane as an internal standard for Gas Chromatography (GC) analysis. The hydrotreating process was conducted in a fixed-bed flow microreactor under the following conditions: the temperature range of 250–340 °C, 1.5 MPa of hydrogen pressure, liquid hourly space velocity of 5 h⁻¹ and volume ratio of hydrogen to feed of 100 N L/L. Liquid products were analyzed by GC method. The catalyst activity was calculated using both the reactants conversions and rate constants of the pseudo-first-order

Scheme 1. Thiophene HDS and *n*-hexene-1 HYDO reactions.

reactions:

$$x_{\text{HDS}} = \frac{C_S^0 - C_S}{C_S^0} \times 100 \text{ and } x_{\text{HYDO}} = \frac{C_{\text{Hexane}}}{C_{\text{Hexene}}} \times 100, \quad (8)$$

Where, x_{HDS} and x_{HYDO} are the HDS and HYDO conversions of thiophene and *n*-hexene-1 (%), respectively; C_S^0 and C_{Hexene}^0 are the thiophene and hexenes (*n*-hexene-1 with its linear isomers) in the feedstock (wt. %), respectively; C_S and C_{Hexane} are the thiophene and *n*-hexane (the only saturated hydrocarbon in the feed) contents in the products (wt. %), respectively;

$$k_{\text{HDS}} = -\frac{F_T}{W} \ln(1 - x_{\text{HDS}}) \text{ and } k_{\text{HYDO}} = -\frac{F_{\text{Hexene}}}{W} \ln(1 - x_{\text{HYDO}}), \quad (9)$$

where k_{HDS} and k_{HYDO} are the pseudo-first order reaction constants of thiophene HDS and *n*-hexene-1 HYDO ($\text{mol g}^{-1} \text{h}^{-1}$), respectively; x_{HDS} and x_{HYDO} are the HDS and HYDO conversions (%), respectively; $F_{\text{H}}(\text{Hexene})$ is the reactant molar flow (mol h^{-1}) and W is the weight of the catalyst (g).

To estimate the selectivity of synthesized catalysts the HDS/HYDO selectivity factor was calculated [43] according to the following equation (Scheme 1):

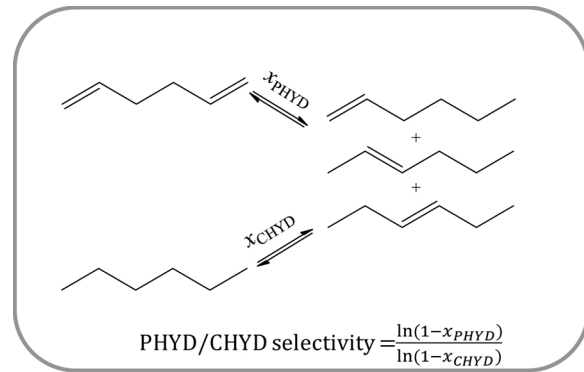
$$\text{HDS/HYDO selectivity} = \frac{\ln(1 - x_{\text{HDS}})}{\ln(1 - x_{\text{HYDO}})} \quad (10)$$

To estimate the productivity of CoMo active sites of synthesized samples the turnover frequency (TOF) numbers were calculated with the following equations:

$$\text{TOF}_{\text{HDS}} = \frac{F_T \cdot x_{\text{HDS}} \cdot 96}{W \cdot C_{\text{MoS}_2} \cdot D \cdot 3600} \text{ and } \text{TOF}_{\text{HYDO}} = \frac{F_{\text{Hexene}} \cdot x_{\text{HYDO}} \cdot 96}{W \cdot C_{\text{MoS}_2} \cdot D \cdot 3600} \quad (11)$$

where F_T and F_{Hexene} are the reactant flows (mol h^{-1}); x_{HDS} and x_{HYDO} are the HDS and HYDO conversions (%), respectively; W is the weight of the catalyst (g); C_{MoS_2} is the effective Mo content in MoS_2 (wt. %) calculated from XPS; D is the dispersion of the active phase species calculated according Eq. (5).

For studying the catalyst performance in selective hydrogenation the model mixture of 5 wt. % of 1,5-hexadiene, 30 wt. % of *n*-heptene-1 and *n*-octane as a solvent was used. The selective hydrogenation process was carried out in a fixed-bed flow microreactor under the following conditions: the temperatures of 250 and 340 °C, 1.5 MPa of hydrogen pressure, liquid hourly space velocity of 3.3 h^{-1} and volume ratio of hydrogen to feed of 100 N L/L. Liquid products were analyzed also by GC method. The reaction of diolefin hydrogenation was proposed as a sequence of two elementary reactions (Scheme 2). The reactions of isomerization of double bonds with formation of diolefins were disregarded. Products of diolefin polymerization were not detected during the experiments. The activity of the catalysts was evaluated using conversion of 1,5-hexadiene (x_{Diene}) and hydrogenation rate of *n*-heptene-1:



Scheme 2. 1,5-Hexadiene hydrogenation route.

$$x_{\text{Diene}} = \frac{C_{1,5-\text{Diene}}^0 - C_{1,5-\text{Diene}}}{C_{1,5-\text{Diene}}^0} \times 100 \text{ and } x_{\text{HYDO}} = \frac{C_{\text{Heptane}}}{C_{\text{Heptene}}} \times 100, \quad (12)$$

where $C_{1,5-\text{Diene}}^0$ and C_{Heptene}^0 are the 1,5-hexadiene and *n*-heptene-1 contents in the feed (mol. %), respectively; $C_{1,5-\text{Diene}}$ and C_{Heptane} are the 1,5-hexadiene and heptane contents in the products (mol. %), respectively.

To estimate the difference between partial and complete hydrogenation of diene the values of integrated selectivity and conversions via partial and complete hydrogenation routes were calculated:

$$\begin{aligned} S_{\text{PHYD}} &= \frac{C_{\text{Hexene}}}{C_{\text{Diene}} + C_{\text{Hexene}} + C_{\text{Hexane}}} \times 100 \text{ and } S_{\text{CHYD}} \\ &= \frac{C_{\text{Hexane}}}{C_{\text{Diene}} + C_{\text{Hexene}} + C_{\text{Hexane}}} \times 100 \end{aligned} \quad (13)$$

where S_{PHYD} and S_{CHYD} are the integrated selectivity of partial and complete hydrogenation of diene, respectively; C_{Hexene} , C_{Hexane} and C_{Diene} are the hexenes, hexane and dienes (excluding 1,5-hexadiene) contents in the products (mol. %), respectively.

$$\begin{aligned} x_{\text{PHYD}} &= \frac{C_{\text{Hexene}} + C_{\text{Hexane}}}{C_{1,5-\text{Diene}}^0} \times 100 \text{ and } x_{\text{CHYD}} = \frac{C_{1,5-\text{Diene}}^0 \cdot x_{\text{PHYD}} - C_{\text{Hexene}}}{C_{1,5-\text{Diene}}^0 \cdot x_{\text{PHYD}}} \\ &\times 100 \end{aligned} \quad (14)$$

where x_{PHYD} and x_{CHYD} are the partial hydrogenation and complete hydrogenation conversions of diene (%), respectively, $C_{1,5-\text{Diene}}^0$ is the 1,5-hexadiene content in the feed (mol. %); C_{Hexene} and C_{Hexane} are the hexenes and hexane contents in the products (mol. %), respectively.

The rate constants of proceeding reactions were calculated using the following equations:

$$\begin{aligned} k_{\text{PHYD}} &= -\frac{F_{1,5-\text{Diene}}}{W} \ln(1 - x_{\text{PHYD}}), \quad k_{\text{CHYD}} \\ &= -\frac{F_{1,5-\text{Diene}} \cdot x_{\text{PHYD}}}{W} \ln(1 - x_{\text{CHYD}}), \quad k_{\text{HYDO}} \\ &= -\frac{F_{\text{Heptene}}}{W} \ln(1 - x_{\text{HYDO}}) \end{aligned} \quad (15)$$

where k_{PHYD} , k_{CHYD} and k_{HYDO} are the pseudo-first order reaction constants of partial and complete hydrogenation of diene and *n*-heptene-1 HYDO ($\text{mol g}^{-1} \text{h}^{-1}$), respectively; x_{PHYD} , x_{CHYD} and x_{HYDO} are the partial hydrogenation and complete hydrogenation conversions of diene and *n*-heptene-1 conversion (%), respectively, F is the reactant molar flow (mol h^{-1}) and W is the weight of the catalyst (g).

To evaluate the selectivity of synthesized samples PHYD/CHYD selectivity was calculated according to the following equation:

$$\text{PHYD/CHYD selectivity} = \frac{\ln(1 - x_{\text{PHYD}})}{\ln(1 - x_{\text{CHYD}})} \quad (16)$$

The TOF values of active sites of synthesized catalysts in proceeding reactions were also calculated in a similar way (11):

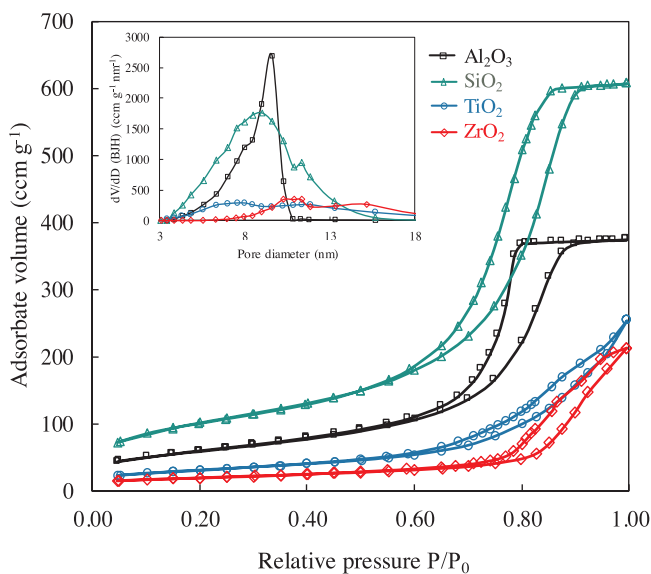


Fig. 1. N_2 adsorption-desorption isotherms for supports.

$$\begin{aligned}
 TOF_{\text{PHYD}} &= \frac{F_{1,5-\text{Diene}} \cdot x_{\text{Diene}} \cdot S_{\text{PHYD}} \cdot 96}{W \cdot C_{\text{MoS}_2} \cdot D \cdot 3600}, \quad TOF_{\text{CHYD}} \\
 &= \frac{F_{1,5-\text{Diene}} \cdot x_{\text{Diene}} \cdot S_{\text{CHYD}} \cdot 96}{W \cdot C_{\text{MoS}_2} \cdot D \cdot 3600} \quad \text{and} \quad TOF_{\text{HYDO}} = \frac{F_{\text{Heptene}} \cdot x_{\text{HYDO}} \cdot 96}{W \cdot C_{\text{MoS}_2} \cdot D \cdot 3600}
 \end{aligned} \quad (17)$$

Where, $F_{1,5-\text{Diene}}$ and F_{Heptene} are the reactant flows (mol h^{-1}); x_{Diene} and x_{HYDO} are the conversions of 1,5-hexadiene and *n*-heptene-1 hydrogenation, respectively; S_{PHYD} and S_{CHYD} are the integrated selectivity of partial and complete hydrogenation; W is the weight of the catalyst (g); C_{MoS_2} is the effective MoS_2 content (wt. %) calculated from XPS; D is the dispersion.

3. Results

3.1. Physical-chemical characterization

The acidity of the used supports differed from each other by the amount of acid sites (Table 1). TiO_2 is characterized by a significant number of acid centers – the amount of desorbed NH_3 was $340 \mu\text{mol/g}$, whereas the acidity of SiO_2 was the lowest. Low-temperature nitrogen adsorption–desorption isotherms for supports are presented in Fig. 1. According to IUPAC classification pores structure of carriers is characterized with isotherm type IV and hysteresis loop of type H2 (for Al_2O_3 and SiO_2) and H4 (for TiO_2 and ZrO_2). Moreover, carriers varied notably in specific surface area and pore size distribution what resulted in differences in textural properties of KCoPMo/Sup catalysts (Table 1). The specific surface area of synthesized samples decreased in the following order: $\text{Al}_2\text{O}_3 > \text{SiO}_2 > \text{TiO}_2 > \text{ZrO}_2$. The pore size distribution also changed after deposition of active phase on the support (Fig. 1S). During the sulfidation process of the catalysts the citric acid transformed to coke species, what resulted in the formation of secondary mesopores with lower sizes. Moreover, the specific surface area of the catalysts significantly decreased in comparison with the initial support due to the coke formation, as well as a great metal loading to the catalysts.

The nature of used support determined the properties of KCoMo active phase due to different interaction degree between carriers and precursors (Fig. 2). The longest linear size of MoS_2 crystallites as well as the highest average stacking number was detected for SiO_2 -supported catalyst and the shortest linear size and the smallest stacking number – for the sample synthesized on the basis of ZrO_2 (Table 2). As the result, the dispersion of K-Co-PMo/ SiO_2 catalyst was the lowest and the active

phase of K-Co-PMo/ ZrO_2 sample was characterized with highly dispersed species. Catalysts synthesized on the basis of TiO_2 and Al_2O_3 were intermediate from the point of the dispersion level. The highest edge-to-corner ratio was observed on K-Co-PMo/ SiO_2 catalyst what could be indicative of great HDS/HYDO selectivity level [7].

The XPS data for sulfided catalysts allowed analyzing the composition and state of all active phase species on the surface of the support. The decomposed Mo3d and Co2p spectra of the synthesized samples are shown in (Fig. 2S). The measured binding energies (BE) are listed in Table 3. The components at 778.9, 778.3 and 781.6 eV were in a good agreement with the literature data for CoMoS active species, CoS_x separate sulfides and Co^{2+} in oxygen surroundings deposited on Al_2O_3 [7,56–58]. Using other supports led to a modest shift less than 1.0 eV towards lower BE for sulfided state of cobalt species what could be attributed to a slight electronic effect of the carrier. The BE of main contributors in molybdenum region for K-Co-PMo/ Al_2O_3 catalysts were also corresponded to the literature data [7,56–58]: at 228.6, 229.8 and 232.0 eV were associated with MoS_2 , $\text{MoS}_{x,y}$ and Mo^{6+} , respectively. For SiO_2 , TiO_2 and ZrO_2 -supported catalysts the BE of main contributors in molybdenum region were similar to those for alumina. The peak at a BE of 161.8 eV were assigned to sulfur ($\text{S} 2p_{3/2}$) in sulfides (S^{2-}) [7,56–58] for Al_2O_3 -supported catalyst. In the sulfur spectra there was also a slight contribution of SO_4^{2-} observed what is ordinary for K-doped TMS catalysts [59]. The same peaks for other catalysts was also observed with slight shift of about 0.4–0.5 eV towards lower energies. For all catalysts the contributions of $\text{K} 2p_{3/2}$ and $\text{P} 2p_{3/2}$ at the ranges of 292.5–293.0 and 132.8–133.8, respectively, were also detected corresponded to K^+ and P^{2+} states [56,59].

The sulfidation degree of the molybdenum was equal for all the samples – relative concentrations of MoS_2 were in the range of 79–83 rel. %. The distribution of Co species on the Al_2O_3 -supported catalyst significantly differed from the other samples: the majority of cobalt atoms decorated crystallites of MoS_2 with the formation of active CoMoS species. In catalysts synthesized on the basis of SiO_2 , TiO_2 and ZrO_2 the selectivity in formation of active phase was not as high as for Al_2O_3 -supported sample – more than a half of cobalt atoms formed the low-active separate sulfides CoS_x . That could be explained by the fact of lower stability of citric complex with Co atoms on the surface of inert supports (SiO_2 , TiO_2 and ZrO_2) that resulted in earlier complex decomposition and sulfidation of promoters before the formation of MoS_2 crystallites.

The XPS analysis allowed determining the effective concentrations of metals on the surface of the catalysts. Earlier we had obtained that high HDS/HYDO selectivity was related to high promotion ratio of active phase edges [57]. The highest promotion ratio of MoS_2 was observed on Al_2O_3 -supported catalyst as well as the great effective content of Co in CoMoS active phase what should determine the highest activity of catalyst [57]. Moreover, from the XPS and HRTEM results the edge-to-corner ratio of the CoMoS₂ slabs was also calculated (Table 2). The highest edge-to-corner ratio of the CoMoS₂ slabs was observed on SiO_2 -supported sample.

TPR-profiles of sulfided K-Co-PMo/Sup catalysts are shown at Fig. 3. The temperature of first reduction peak attributed to the edge sulfur reduction and indirectly indicated the reactivity of active sites, whereas the peak area referred to the amount of active centers [60,61]. According to the TPR results the Mo-S bond strength increased in the following range:

$$\text{SiO}_2 (301^\circ\text{C}) < \text{TiO}_2 (345^\circ\text{C}) < \text{ZrO}_2 (373^\circ\text{C}) < \text{Al}_2\text{O}_3 (387^\circ\text{C}).$$

At the same time the number of active centers in K-Co-PMo/ Al_2O_3 was the highest in comparison with other samples and for SiO_2 -supported catalyst the content of active sites with the high reactivity was the lowest.

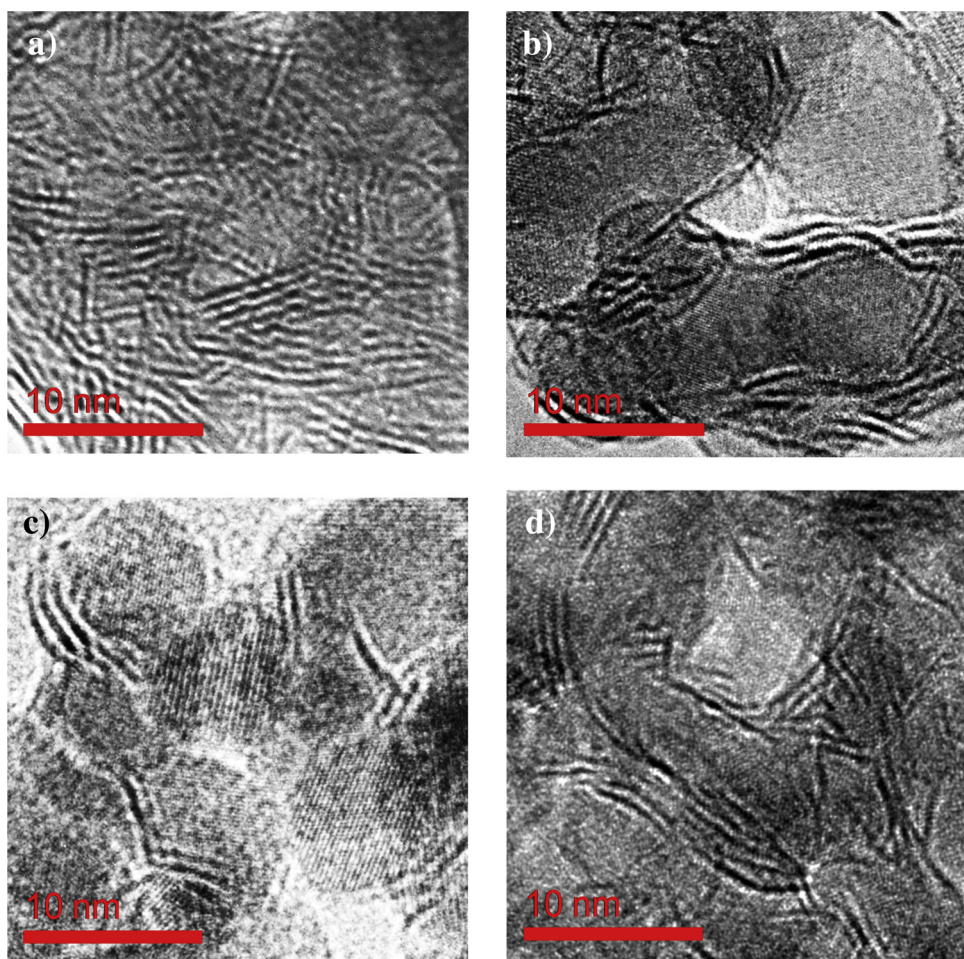


Fig. 2. HRTEM images of prepared K-Co-PMo/Sup catalysts (a-SiO₂, b-TiO₂, c-ZrO₂, d-Al₂O₃).

3.2. Catalytic properties in hydrotreating of model FCC gasoline

The catalytic properties of synthesized K-Co-PMo/Sup catalysts in hydrotreating of model FCC gasoline are presented in the Table 5. At the process temperature of 250 °C the most active sample in HDS as well as in HYDO was TiO₂-supported one (rate constants were 9.5×10^{-5} and $865 \times 10^{-5} \text{ mol} \text{ h}^{-1} \text{ g}^{-1}$, respectively). K-Co-PMo/Al₂O₃ catalyst was two times less active in HDS and about three times less active in HYDO. As the result, the HDS/HYDO selectivity of Al₂O₃-supported sample was higher than the same for the catalyst synthesized using TiO₂ (2.5 compared to 1.5). The HDS rate constants of SiO₂- and ZrO₂-supported catalysts were equal to $0.9 \times 10^{-5} \text{ mol} \text{ h}^{-1} \text{ g}^{-1}$, whereas the HYDO rate constant of K-Co-PMo/ZrO₂ catalyst was three times higher than HYDO activity of SiO₂-supported sample (62×10^{-5} compared to $21 \times 10^{-5} \text{ mol} \text{ h}^{-1} \text{ g}^{-1}$). Hence the highest HDS/HYDO selectivity was obtained for KCoMoS active phase deposited on SiO₂ as a carrier.

The dependence, similar to the rate constants, was observed for TOF

values of synthesized catalysts (Table 1S). The highest productivity of active sites in HDS and HYDO reactions was obtained at TiO₂-supported catalyst (1.14×10^{-4} and $110 \times 10^{-4} \text{ s}^{-1}$, respectively). K-Co-PMo/Al₂O₃ sample showed moderate TOF numbers: about 1.5 times lower for HDS and 2.0 times lower for HYDO activities in comparison with TiO₂-supported catalyst. The HYDO TOF value of K-Co-PMo/ZrO₂ sample as well as the rate constant was higher than the same value for K-Co-PMo/SiO₂ catalyst, whereas the TOF number in HDS reaction for ZrO₂-supported sample was close to SiO₂-supported one (the rate constants in HDS for two catalysts were also equal).

For all catalysts the temperature dependence of HDS and HYDO conversions was obtained (Fig. 4a). With the temperature rising both HDS and HYDO activities naturally increased for all catalysts. In all temperature range K-Co-PMo/TiO₂ catalyst showed the highest conversion levels, whereas SiO₂- and ZrO₂-supported once exhibited low and close to each other activities. Linearization of relations between HDS and HYDO rate constants and process temperature in Arrhenius

Table 2

Morphological characteristics of the KCoMoS active phase species calculated from HRTEM micrographs of sulfided K-Co-PMo/Sup catalysts.

Catalyst	Average length L° (nm)	Average stacking number N°	Dispersion of KCoMoS particles D^{a}	$(f_e/f_c)_{\text{Mo}}^{\text{b}}$	$(f_e/f_c)_{\text{CoMo}}^{\text{c}}$
K-Co-PMo/SiO ₂	6.2	2.2	0.20	8.2	10.6
K-Co-PMo/TiO ₂	4.7	1.7	0.25	5.8	7.4
K-Co-PMo/ZrO ₂	3.8	1.5	0.31	4.4	6.0
K-Co-PMo/Al ₂ O ₃	4.0	1.8	0.29	4.8	6.8

^bEdge-to-corner ratio of MoS₂ slab calculated from HRTEM data (Eq. (8)).

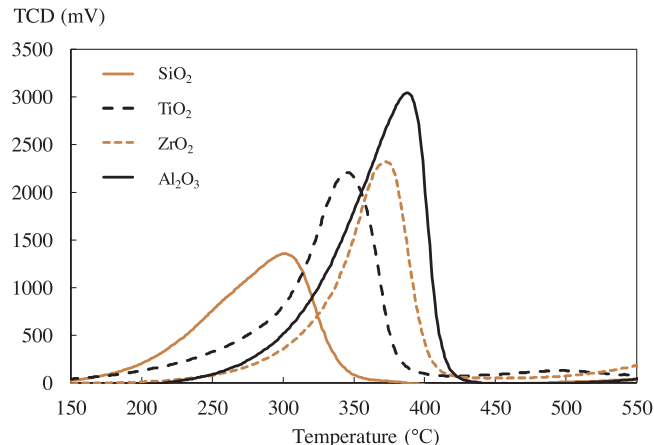
^cEdge-to-corner ratio of CoMoS slab calculated from HRTEM and XPS data (Eq. (13)).

^aMoS₂ dispersion calculated using HRTEM data (Eq. (11)).

Table 3

Binding energies (eV) measured by XPS for cobalt, molybdenum and sulfur species present at the surface of sulfided K-Co-PMo/Sup catalysts.

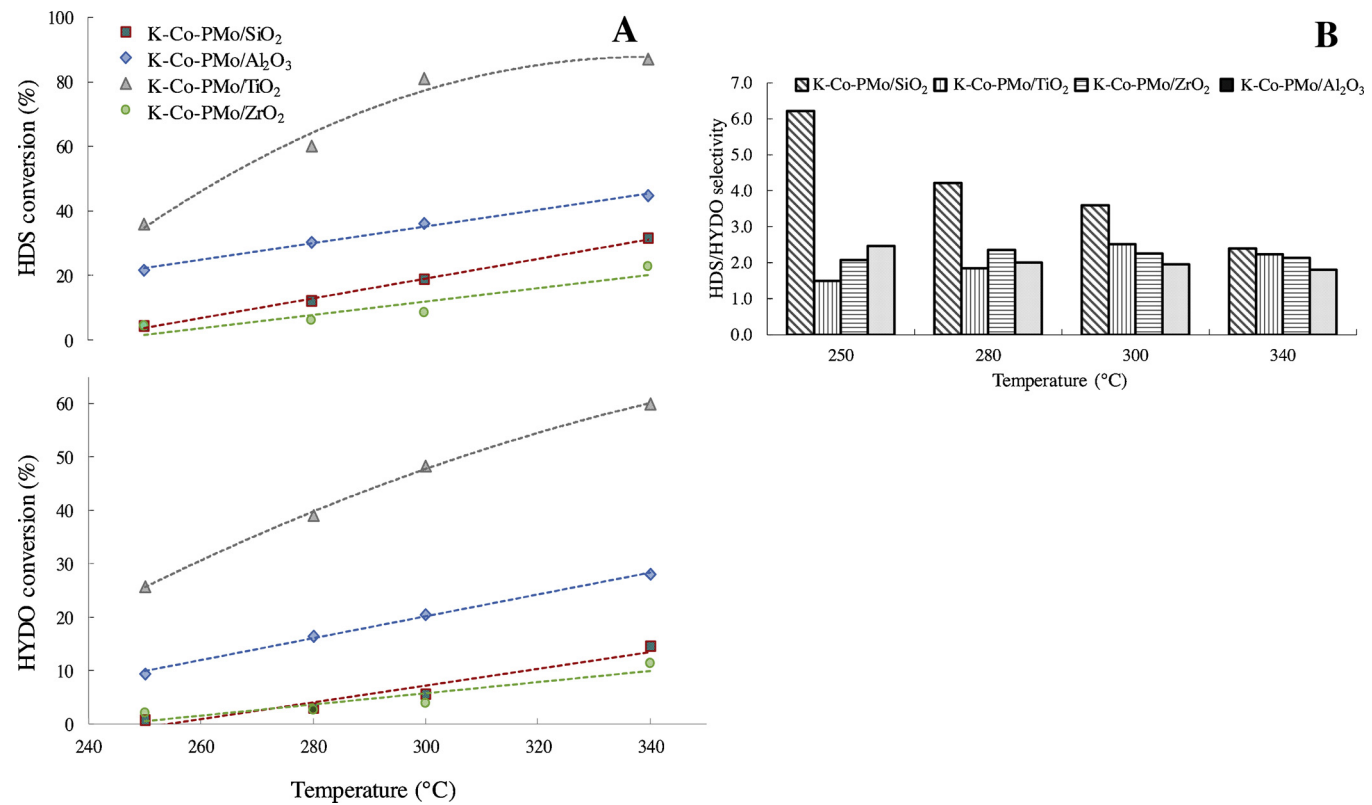
Catalyst	Co 2p _{3/2}			Mo 3d _{5/2}			S 2p _{3/2}	K 2p _{3/2}	P 2p _{3/2}
	CoMoS	Co ₉ S ₈	Co ²⁺	MoS ₂	MoS _x O _y	Mo ⁶⁺	S ²⁻	K ⁺	P ⁵⁺
K-Co-PMo/SiO ₂	778.4	777.9	781.8	228.5	229.8	232.0	161.4	293.0	133.3
K-Co-PMo/TiO ₂	778.3	777.4	781.7	228.5	229.9	232.0	161.3	292.5	132.8
K-Co-PMo/ZrO ₂	778.3	777.5	781.8	228.6	229.8	232.0	161.4	292.8	133.1
K-Co-PMo/Al ₂ O ₃	778.9	778.3	781.6	228.6	229.8	232.0	161.8	292.9	133.8

**Fig. 3.** TPR profiles for sulfided K-Co-PMo/Sup catalysts.

plot coordinates (Fig. 3S) allowed calculating apparent activation energies $E_A^{\#}$ and pre-exponential factor $\ln A$ (Table 5). The highest $E_A^{\#}$ values in HDS as well as in HYDO reactions were obtained at K-Co-PMo/SiO₂ catalyst (63.7 and 91.5 kJ/mol, respectively). The lowest

apparent activation energy in HDS was detected over Al₂O₃-supported sample (29.8 kJ/mol) and in HYDO – at TiO₂-supported catalyst (33.4 kJ/mol). At the same time the highest pre-exponential factors in HDS and HYD were detected at SiO₂-supported catalyst (13.3 and 17.9, respectively) indicated the greatest number of active centers with low strength and the lowest pre-exponential factors in HDS and HYD were obtained on K-Co-PMo/Al₂O₃ catalyst (7.0 and 7.5, respectively) exhibited the lower amount of active sites with high strength. Since all the catalysts were represented by CoMoS active phase modified by potassium and were characterized with approximate pore size distributions (without micropores and with the ratio of pores in the range of 2–4 nm less than 10%) the differences in kinetic characteristics could be explained by support effect in particular the acidity of the carrier materials, isoelectric point and the interaction strength between active phase species and the support (Table 1), but not by active phase composition itself or diffusion limitations. Changing the strength of HDS and HYDO active sites directly connected to decreasing of apparent activation energy from SiO₂ to Al₂O₃-supported catalysts.

The HDS/HYDO selectivity of synthesized catalysts differed a lot, depending on the type of used carrier (Table 5, Fig. 4b). With the temperature rise selectivity of ZrO₂- and TiO₂-supported catalysts passed through maximum, whereas for samples synthesized using SiO₂ and Al₂O₃ the HDS/HYDO selectivity decrease was detected. At high

**Fig. 4.** a Dependence of HDS and HYDO activity in HDT of a mixture of thiophene and *n*-hexene-1 on the process temperature for K-Co-PMo/Sup catalysts. b Dependence of HDS/HYDO selectivity in HDT of a mixture of thiophene and *n*-hexene-1 on the process temperature for K-Co-PMo/Sup catalysts.

process temperature the values of HDS/HYDO selectivity for different catalysts were close to each other whereas at 250 °C SiO₂-supported sample surpassed other catalysts at HDS/HYDO selectivity level.

3.3. Catalytic properties in selective hydrogenation of diolefin

The results of selective hydrogenation of a mixture of 1,5-hexadiene and *n*-heptene-1 are summarized in Table 6. The highest activity in diene conversion (including reactions of hydrogenation and double-bond isomerization), as well as in hydrogenation of one double bond was obtained at K-Co-PMo/TiO₂ catalyst (rate constant was $39.8 \times 10^{-4} \text{ mol h}^{-1} \text{s}^{-1}$) and the lowest – at SiO₂-supported sample (rate constant was $18.3 \times 10^{-4} \text{ mol h}^{-1} \text{s}^{-1}$). At the same time the most active catalyst in hydrogenation of forming olefins to paraffin (complete hydrogenation of diolefin) was also K-Co-PMo/SiO₂ sample – rate constants of partial hydrogenation and complete hydrogenation were close to each other and majority part of generated hexenes was further reduced to hexane. Another curios observation is that the most active catalyst in *n*-heptene-1 hydrogenation (Al₂O₃-supported sample) was less active in complete hydrogenation of hexenes and vice versa (rate constants of olefin hydrogenation and complete hydrogenation of diolefin at K-Co-PMo/SiO₂ catalyst were 1.5×10^{-4} and $12.7 \times 10^{-4} \text{ mol h}^{-1} \text{s}^{-1}$, respectively). Integrated selectivity shows the part of hexenes (S_{PHYD}) and hexane (S_{CHYD}) in the reaction products. For TiO₂-, ZrO₂- and Al₂O₃-supported catalysts the integrated selectivities were close to each other whereas for sample synthesized on silica the fraction of hexane was much higher than hexenes amount. PHYD/CHYD selectivity of synthesized samples depended on the type of using carrier. The better selectivity level was obtained at TiO₂-supported catalyst – about 5.6, while the PHYD/CHYD selectivity of K-Co-PMo/SiO₂ catalyst was below 1 indicated prevalence of complete hydrogenation reactions under partial hydrogenation.

K-Co-PMo/TiO₂ sample possessed the better productivity of active sites (Table 1S) in partial hydrogenation of diolefin and low productivity in further hydrogenation of forming olefins (25×10^{-4} and $6 \times 10^{-4} \text{ s}^{-1}$, respectively). The lowest productivity in complete hydrogenation was detected at Al₂O₃-supported catalyst ($5 \times 10^{-4} \text{ s}^{-1}$). The TOF number of complete diolefin hydrogenation at K-Co-PMo/SiO₂ catalyst was the highest ($21 \times 10^{-4} \text{ s}^{-1}$) among other samples.

4. Discussion

Recently we obtained several structure-to-property correlations for K- and non-modified TMS catalysts for selective hydrotreating of FCC gasoline [7,57]. It was found that high level of HDS/HYDO selectivity was connected to the great average slab length of active phase crystallites as well as high Co/Mo promotion ratio of slab edges. Moreover, high selectivity was also related to high ratio of amount of edge's Co atoms to the amount of corner's Co atoms.

To understand if there was any effect of the nature of the carrier on the productivity of active sites, or it was only due to geometrical characteristics of active phase species, the 3D dependencies of TOF numbers in thiophene HDS and *n*-hexene-1 HYDO over K-Co-PMo/Sup and K_x-Co-PMo/Al₂O₃ [7] catalysts on the average slab length and stacking number of the CoMoS₂ crystallites were plotted (Fig. 5). Activity of the samples supported on Al₂O₃ and SiO₂ well correlated with activity of catalysts supported on alumina with different amount of potassium – high TOF values obtained at lower average slab length and stacking number, increasing of the linear size of active phase crystallites and the number of stacks per slab led to decrease of TOF numbers in thiophene HDS as well as olefin HYDO. K-Co-PMo/TiO₂ catalyst showed extremely high productivity of active sites in both types of the reactions. With the DFT modeling P. Raybaud and co-workers [62] established that an epitaxial relation appeared between Mo-edge of MoS₂ crystallites and the surface of TiO₂. As the result of this active phase supported on TiO₂ was represented by sulfur-deficient particles

with higher ratio of Mo-edge to S-edge in comparison with alumina what caused an advanced activity. Later, during DFT modeling of CoMoS active phase species supported on alumina and anatase P. Raybaud and coworkers [63] showed that a significantly higher S-edge/Mo-edge ratio on Al₂O₃ favored optimal Co decoration that also conformed to results of XPS (Table 4) – the relative amount of CoMoS phase 2 times lower at TiO₂-supported catalysts in comparison with Al₂O₃-supported one. At the same time the values of TOF numbers for the sample synthesized on the basis of TiO₂ contradicted to the results obtained for non-modified CoMo/TiO₂ system in the literature, what could be connected with the following explanation. Promoting MoS₂ clusters with Co destabilized epitaxial relationship on anatase that resulted in getting less amount of non-anchored edge active sites on TiO₂ in comparison with Al₂O₃. Modifying active phase species with potassium led to formation of more electron-deficient KCoMoS sites [64] that could favor changing of the adhesion energies between support and the active phase particles, and as the result – changing in productivity of active sites. Nevertheless, there are several investigations showed the better activity of CoMo/TiO₂ catalyst in HDS reactions compared to CoMo/Al₂O₃ sample [24,65]. Low productivity of ZrO₂-supported catalyst is also in the line with open source publication [66–68].

The dependence of HDS/HYDO selectivity on the ratio of the number of edge's to corner's Co atoms for K-Co-PMo/Sup and K_x-Co-PMo/Al₂O₃ [7] catalysts is depicted on Fig. 6. The selectivity of ZrO₂-, SiO₂- and Al₂O₃-supported catalysts good correlated with K_x-Co-PMo/Al₂O₃ samples ($R^2 = 0.93$) indicated the similarity in nature of HDS and HYDO active sites, obtained on three different carriers. On the contrary, the HDS/HYDO selectivity of TiO₂-supported catalyst was much lower than it could be expected from the value of $(f_e/f_c)_{\text{CoMo}}$, which indicates that active sites of K-Co-PMo/TiO₂ sample differed from active sites of ZrO₂-, SiO₂- and Al₂O₃-supported catalysts.

To define the impact of the nature of the support on activity of K-Co-PMo/Sup catalysts in diolefin selective hydrogenation the 3D dependences of TOF numbers vs. f_e/f_c and temperature of maximum peak reduction obtained from TPR were plotted (Fig. 7). The productivity of active sites in partial hydrogenation of diolefin (reaction 1 at Scheme 2) passed through the maximum when the TOF numbers in complete hydrogenation (reaction 2 at Scheme 2) depended linear both on the ratio of the amount of edge's active sites to the amount of corner's active sites and on the temperature of maximum peak reduction. High values of TOF numbers in complete hydrogenation were obtained both at low temperature of peak reduction maximum and high value of f_e/f_c indicated the active phase presented by large part of edge sites with labile sulfur and low values of TOF numbers in complete hydrogenation were detected at high temperature of peak reduction maximum and low value of f_e/f_c referred to active phase presented by moderate part of edge sites with high energy of Mo-S bond. The most reactive active sites in diolefin partial hydrogenation were detected at K-Co-PMo/TiO₂ catalyst with moderate temperature of peak reduction maximum and medium ratio of edge-to-corner active sites. It is interesting that the temperature of peak reduction maximum well correlated with the acidity of the supports measured by NH₃-TPD pointing out that the nature of used carriers is one of the key factors in the formation of KCoMoS active phase with different selectivity.

Since the catalyst for hydrotreating of FCC gasoline supposed to be highly selective towards HDS reactions and possessed low activity in olefin hydrogenation as much as possible, it is logical to assume that such catalyst will be also selective in partial hydrogenation of diolefin. For that purpose, the dependence of PHYD/CHYD selectivity on HDS/HYDO selectivity was plotted (Fig. 8). The higher HDS/HYDO selectivity the lower PHYD/CHYD selectivity and vice versa. Thus, it is impossible to carry out selective hydrotreating of FCC gasoline and selective hydrogenation of diolefins in FCC gasoline simultaneously on one catalyst, for each process it should be selected the most appropriate catalytic system with desired selectivity.

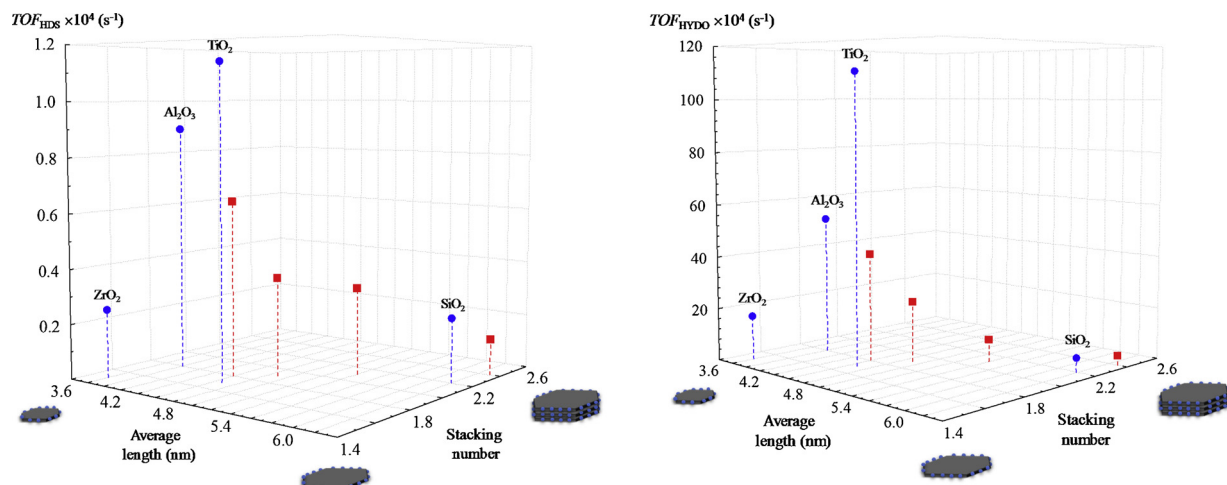


Fig. 5. 3D dependence of the TOF number in thiophene HDS and n-hexene-1 HYDO over K-Co-PMo/Sup (•) and K_x(Co)Mo/Al₂O₃ [7] (■) catalysts on the average length and stacking number of the (Co)MoS₂ phase species.

Table 4

Metal distribution for cobalt and molybdenum species present at the surface of sulfided K-Co-PMo/Sup catalysts.

Catalyst	(Co/Mo) _{slab} ^a	(Co/Mo) _{edge} ^b	C _{CoMoS} ^c (wt. %)	Co distribution (rel. %)			Mo distribution (rel. %)		
				CoMoS	Co ₉ S ₈	Co ²⁺	MoS ₂	MoS _x O _y	Mo ⁶⁺
K-Co-PMo/SiO ₂	0.25	1.3	0.85	37	54	9	79	12	9
K-Co-PMo/TiO ₂	0.33	1.3	1.42	34	54	13	83	9	8
K-Co-PMo/ZrO ₂	0.41	1.4	0.81	32	57	11	80	11	9
K-Co-PMo/Al ₂ O ₃	0.42	1.4	1.29	60	17	23	79	9	12

^a Co/Mo ratio in the CoMoS slabs calculated from XPS results (Eq. (11)).

^b Co/Mo ratio in the CoMoS edges calculated from XPS and HRTEM results (Eq. (10)).

^c Effective Co content in total CoMoS phase species calculated from XPS results (Eq. (12)).

Table 5

Catalytic properties of prepared K-Co-PMo/Sup catalysts in HDT of a mixture of thiophene and n-hexene-1 T = 250 °C, P = 1.5 MPa, LHVS = 5 h⁻¹, H₂/feed = 100 nL/L).

Catalyst	Conversions (%)		Rate constant × 10 ⁵ (mol h ⁻¹ s ⁻¹)		E _A [#] ^a (kJ mol ⁻¹)		lnA ^a		Selectivity factor HDS/HYDO
	HDS	HYDO	k _{HDS}	k _{HYDO}	HDS	HYDO	HDS	HYDO	
K-Co-PMo/SiO ₂	4	1	0.9	21	63.7 ± 0.7	91.5 ± 0.8	13.3 ± 0.2	17.9 ± 0.2	6.2
K-Co-PMo/TiO ₂	36	26	9.5	865	46.5 ± 0.9	33.4 ± 0.3	11.6 ± 0.2	8.1 ± 0.1	1.5
K-Co-PMo/ZrO ₂	4	2	1.0	62	54.4 ± 0.9	53.2 ± 1.1	10.7 ± 0.2	9.7 ± 0.2	2.1
K-Co-PMo/Al ₂ O ₃	22	9	5.5	302	29.8 ± 0.3	35.5 ± 0.4	7.0 ± 0.1	7.5 ± 0.1	2.5

^a Apparent activation energies and pre-exponential factors were calculated in the temperature range of 250–340 °C.

Table 6

Catalytic properties of prepared K-Co-PMo/Sup catalysts in selective hydrogenation of mixture of hexadiene-1,5 and heptene-1 (T = 250 °C, P = 1.5 MPa, LHVS = 3.3 h⁻¹, H₂/feed = 100 nL/L).

Catalyst	Conversions (%)				Rate constant × 10 ⁴ (mol h ⁻¹ g ⁻¹)			Integrated selectivity		PHYD/CHYD selectivity
	Diene	PHYD	CHYD	HYDO	k _{PHYD}	k _{CHYD}	k _{HYDO}	S _{PHYD}	S _{CHYD}	
K-Co-PMo/SiO ₂	52	31	56	1	18.3	12.7	1.5	0.26	0.32	0.4
K-Co-PMo/TiO ₂	93	77	23	9	39.8	5.4	13.1	0.66	0.17	5.6
K-Co-PMo/ZrO ₂	47	40	25	5	14.1	3.2	10.5	0.66	0.20	1.8
K-Co-PMo/Al ₂ O ₃	60	49	22	10	18.1	3.3	14.3	0.66	0.17	2.7

5. Conclusions

The type of used carrier (Al₂O₃, SiO₂, ZrO₂ and TiO₂) significantly affected the morphology of active phase as well as catalytic properties in selective hydrotreating of model FCC gasoline and selective hydrogenation of diolefins.

K-Co-PMo/TiO₂ sample showed the highest activity in both HDS

and HYDO reactions with the lowest HDS/HYDO selectivity simultaneously. On the contrary SiO₂-supported catalyst possessed lowest activity in hydrotreating of FCC gasoline and highest HDS/HYDO selectivity. KCoMoS active phase deposited on alumina exhibited good balanced activity and HDS/HYDO selectivity.

In partial hydrogenation of diolefin the most active and selective catalyst was also TiO₂-supported one. And the lowest selectivity in

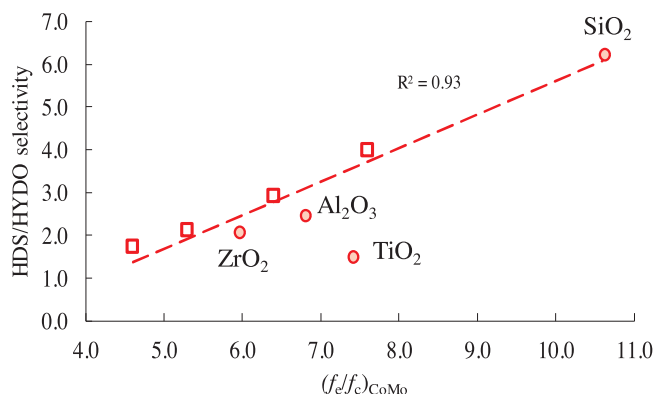


Fig. 6. The dependence of HDS/HYDO selectivity in HDT of a mixture of thiophene and n-hexene-1 from the ratio of the number of edge's to corner's Co atoms for K-Co-PMo/Sup and K_x-Co-PMo/Al₂O₃ [7] catalysts.

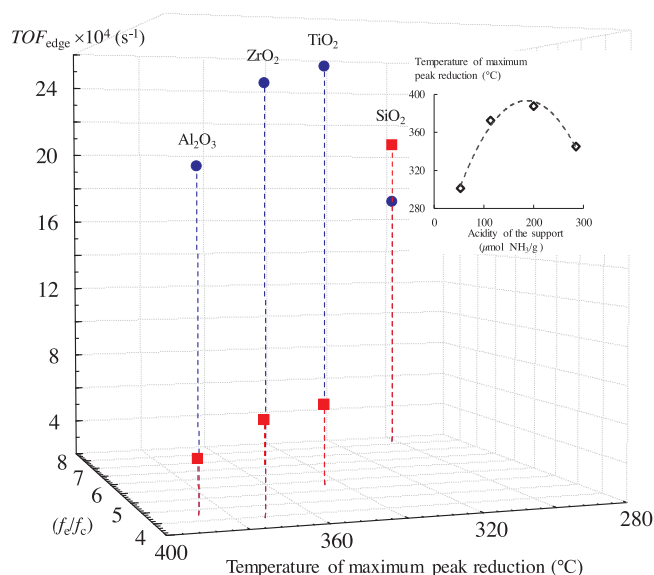


Fig. 7. 3D dependence of the TOF numbers in diolefin partial hydrogenation (•) and diolefin complete hydrogenation (■) over K-Co-PMo/Sup catalysts on the ratio of the amount of edge's active sites to the amount of corner's active sites and temperature of maximum peak reduction for samples in TPR measurements. Temperature of maximum peak reduction for K-Co-PMo/Sup catalysts vs. the acidity of the supports.

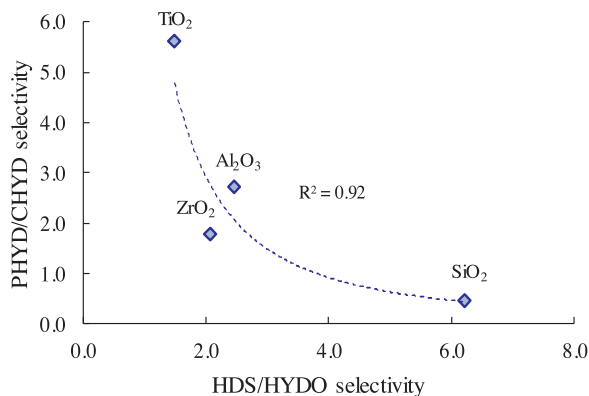


Fig. 8. The dependence of HDS/HYDO selectivity in hydrotreating of model FCC gasoline on PHYD/CHYD selectivity in hydrogenation of diolefin over K-Co-PMo/Sup catalysts.

partial hydrogenation as well as the lowest activity was obtained at K-Co-PMo/SiO₂ sample.

In favor of great impact of support properties (acidity and interaction strength between active phase species and carrier) on catalytic characteristics of active KCoMoS phase the following points are indicating:

- the longest linear size of MoS₂ crystallites, as well as the highest average stacking number were detected for SiO₂-supported catalyst and the shortest linear size and the smallest stacking number – for the sample synthesized on the basis of ZrO₂, TiO₂- and Al₂O₃-supported samples were intermediate from the point of the dispersion level.
- the selectivity of formation of active CoMoS phase at K-Co-PMo/Al₂O₃ catalyst was high whereas for other samples it was low – more than a half of cobalt atoms formed the low-active separate sulfides CoS_x.
- the highest apparent activation energies both in HDS and HYDO reactions were obtained at K-Co-PMo/SiO₂ catalyst. The lowest $E_A^\#$ values in HDS was detected over Al₂O₃-supported sample and in HYDO – at TiO₂-supported one.
- good correlation between productivity of active centers in reactions of selective hydrogenation of diolefin and maximum peak reduction obtained from TPR, which in turn depended on acidity of using supports.

Selectivities in two processes – hydrotreating and diolefin hydrogenation – depended on each other inversely: the highest HDS/HYDO selectivity attributed to low level of PHYD/CHYD selectivity and consequently high activity in undesirable complete hydrogenation of diolefins. In other words, it is impossible to carry out selective hydrotreating of FCC gasoline and selective hydrogenation of diolefins in FCC gasoline simultaneously on one catalyst. For each process the most appropriate catalytic system with desired selectivity should be selected.

Declaration of Competing Interest

The authors declare that they have no known competing financial interests or personal relationships that could have appeared to influence the work reported in this paper.

Acknowledgments

The work was financially supported by The Russian Science Foundation (project No 17-73-10446).

Appendix A. Supplementary data

Supplementary material related to this article can be found, in the online version, at doi:<https://doi.org/10.1016/j.apcatb.2019.118041>.

References

- [1] BP Energy Outlook, edition, (2019).
- [2] S. Brunet, D. Mey, G. Perot, C. Bouchy, F. Diehl, On the hydrodesulfurization of FCC gasoline: a review, *Appl. Catal. A Gen.* 278 (2005) 143–172.
- [3] D. Mey, S. Brunet, C. Canaff, F. Maugé, C. Bouchy, F. Diehl, HDS of a model FCC gasoline over a sulfided CoMo/Al₂O₃ catalyst: effect of the addition of potassium, *J. Catal.* 227 (2004) 436–447, <https://doi.org/10.1016/j.jcat.2004.07.013>.
- [4] D. Mey, S. Brunet, G. Perot, F. Diehl, Catalytic deep HDS of model FCC feed over a CoMo/Al₂O₃ catalyst modified by potassium, *Am. Chem. Soc. Prepr. Fuel Chem.* 48 (2003) 44.
- [5] Y. Fan, J. Lu, G. Shi, H. Liu, X. Bao, Effect of synergism between potassium and phosphorus on selective hydrodesulfurization performance of Co-Mo/Al₂O₃ FCC gasoline hydro-upgrading catalyst, *Catal. Today* 125 (2007) 220–228, <https://doi.org/10.1016/j.cattod.2007.02.022>.
- [6] Y. Fan, G. Shi, H. Liu, X. Bao, Morphology tuning of supported MoS₂ slabs for selectivity enhancement of fluid catalytic cracking gasoline hydrodesulfurization catalysts, *Appl. Catal. B Environ.* 91 (2009) 73–82, <https://doi.org/10.1016/j.apcatb.2009.07.013>.

apcatb.2009.05.008.

[7] D. Ishutenko, P. Nikulshin, A. Pimerzin, Relation between composition and morphology of K(Co)MoS active phase species and their performances in hydrotreating of model FCC gasoline, *Catal. Today* 271 (2016) 16–27, <https://doi.org/10.1016/j.cattod.2015.11.025>.

[8] P. Nikulshin, D. Ishutenko, Y. Anashkin, A. Mozhaev, A. Pimerzin, Selective hydrotreating of FCC gasoline over KCoMoP/Al₂O₃ catalysts prepared with H₃PMo₁₂O₄₀: effect of metal loading, *Fuel* 182 (2016) 632–639, <https://doi.org/10.1016/j.fuel.2016.06.016>.

[9] A. Yadav, V. Kagdiyal, A. Arun, M.B. Patel, A.A. Gupta, B. Basu, HPLC method for monitoring the conjugated dienes and olefins in FCC, coker gasolines, and their hydrogenated products, *J. Liq. Chromatogr. Relat. Technol.* 38 (2015) 840–846, <https://doi.org/10.1080/10826076.2014.968663>.

[10] Refining processes 2000, *Hydroc. Proc.* 79 (11) (2000) 85–142.

[11] C. Fragale, M. Gargano, N. Ravasio, M. Rossi, I. Santo, V. Amendola, Selective hydrogenation of penta-1,3-diene and cyclooctadienes catalyzed by silver-modified palladium catalysts, *J. Mol. Catal.* 24 (1984) 211–216, [https://doi.org/10.1016/0304-5102\(84\)85132-9](https://doi.org/10.1016/0304-5102(84)85132-9).

[12] B.K. Furlong, J.W. Hightower, T.Y.L. Chan, A. Sarkany, L. Guczi, 1,3-butadiene selective hydrogenation over Pd/alumina and CuPd/alumina catalysts, *Appl. Catal. A Gen.* 117 (1994) 41–51, [https://doi.org/10.1016/0926-860X\(94\)80157-6](https://doi.org/10.1016/0926-860X(94)80157-6).

[13] A.B. Gaspar, G.R. dos Santos, R. de Souza Costa, M.A.P. da Silva, Hydrogenation of synthetic PYGAS-Effects of zirconia on Pd/Al₂O₃, *Catal. Today* 133–135 (2008) 400–405, <https://doi.org/10.1016/j.cattod.2007.12.058>.

[14] Z. Zhou, T. Zeng, Z. Cheng, W. Yuan, Kinetics of selective hydrogenation of pyrolysis gasoline over an egg-shell catalyst, *Chem. Eng. Sci.* 65 (2010) 1832–1839, <https://doi.org/10.1016/j.ces.2009.11.028>.

[15] R.G. Tailleur, J.R. Nascar, Effect of H₂S on selective hydrogenation of diolefins using NiPdCe(x)/Si-Al-coated structured packing catalyst, *Appl. Catal. A Gen.* 439–440 (2012) 125–134, <https://doi.org/10.1016/j.apcata.2012.06.046>.

[16] X. Wen, R. Li, Y. Yang, J. Chen, F. Zhang, An egg-shell type Ni/Al₂O₃ catalyst derived from layered double hydroxides precursor for selective hydrogenation of pyrolysis gasoline, *Appl. Catal. A Gen.* 468 (2013) 204–215, <https://doi.org/10.1016/j.apcata.2013.08.040>.

[17] P. Castaño, B. Pawelec, J.L.G. Fierro, J.M. Arandes, J. Bilbao, Enhancement of pyrolysis gasoline hydrogenation over Pd-promoted Ni/SiO₂/Al₂O₃ catalysts, *Fuel* 86 (2007) 2262–2274, <https://doi.org/10.1016/j.fuel.2007.01.020>.

[18] Y. Qian, S. Liang, T. Wang, Z. Wang, W. Xie, X. Xu, Enhancement of pyrolysis gasoline hydrogenation over Zn- and Mo-promoted Ni/γ-Al₂O₃ catalysts, *Catal. Commun.* 12 (2011) 851–853, <https://doi.org/10.1016/j.catcom.2011.02.006>.

[19] B.W. Hoffer, R.L.C. Bonné, A.D. Van Langeveld, C. Griffiths, C.M. Lok, J.A. Moulijn, Enhancing the start-up of pyrolysis gasoline hydrogenation reactors by applying tailored ex situ presulfidized Ni/Al₂O₃ catalysts, *Fuel* 83 (2004) 1–8, [https://doi.org/10.1016/S0016-2361\(03\)00210-2](https://doi.org/10.1016/S0016-2361(03)00210-2).

[20] E.J.M. Hensen, P.J. Kooyman, Y. Van der Meer, A.M. Van der Kraan, V.H.J. De Beer, J.A.R. Van Veen, R.A. Van Santen, P.J. Kooyman, Y. Van der Meer, A.M. Van der Kraan, The relation between morphology and hydrotreating activity for supported MoS₂ particles, *J. Catal.* 199 (2001) 224–235, <https://doi.org/10.1006/jcat.2000.3158>.

[21] M. Breyses, P. Afanasiev, C. Geantet, M. Vrinat, Overview of support effects in hydrotreating catalysts, *Catal. Today* 86 (2003) 5–16, [https://doi.org/10.1016/S0920-5861\(03\)00400-0](https://doi.org/10.1016/S0920-5861(03)00400-0).

[22] F. Trejo, M.S. Rana, J. Ancheyta, A. Rueda, Hydrotreating catalysts on different supports and its acid-base properties, *Fuel* 100 (2012) 163–172, <https://doi.org/10.1016/j.fuel.2012.04.026>.

[23] F. Trejo, M.S. Rana, J. Ancheyta, S. Chávez, Influence of support and supported phases on catalytic functionalities of hydrotreating catalysts, *Fuel* 138 (2014) 104–110, <https://doi.org/10.1016/j.fuel.2014.02.032>.

[24] T.K.T. Ninh, D. Laurenti, E. Leclerc, M. Vrinat, Support effect for CoMoS and CoNiMoS hydrosulfurization catalysts prepared by controlled method, *Appl. Catal. A Gen.* 487 (2014) 13.

[25] J. Ancheyta, M.S. Rana, E. Furimsky, Hydroprocessing of heavy petroleum feeds: tutorial, *Catal. Today* 109 (2005) 3–15, <https://doi.org/10.1016/j.cattod.2005.08.025>.

[26] L. Kaluža, M. Zdražil, N. Žilková, J. Čejka, High activity of highly loaded MoS₂ hydrosulfurization catalysts supported on organised mesoporous alumina, *Catal. Commun.* 3 (2002) 151–157, [https://doi.org/10.1016/S1566-7367\(02\)00073-0](https://doi.org/10.1016/S1566-7367(02)00073-0).

[27] N. Bejenaru, C. Lancelot, P. Blanchard, C. Lamonié, L. Rouleau, E. Payen, F. Dumeignil, S. Royer, Synthesis, characterization, and catalytic performances of novel CoMo hydrosulfurization catalysts supported on mesoporous aluminas, *Chem. Mater.* 21 (2009) 522–533, <https://doi.org/10.1021/cm802084e>.

[28] X.M. Liu, H.X. Xue, X. Li, Z.F. Yan, Synthesis and hydrosulfurization performance of hierarchical mesoporous alumina, *Catal. Today* 158 (2010) 446–451, <https://doi.org/10.1016/j.cattod.2010.06.032>.

[29] Y. Saito, M. Nagata, T. Funamoto, Y. Masuyama, K. Segawa, Ultra deep hydrosulfurization of dibenzothiophene derivatives over NiMo/TiO₂/Al₂O₃ catalysts, *Appl. Catal. A Gen.* 295 (2005) 11–22, <https://doi.org/10.1016/j.apcata.2005.07.024>.

[30] J. Ramírez, G. Macías, L. Cedeño, A. Gutiérrez-Alejandre, R. Cuevas, P. Castillo, The role of titania in supported Mo, CoMo, NiMo, and NiW hydrosulfurization catalysts: analysis of past and new evidences, *Catal. Today* 98 (2004) 19–30, <https://doi.org/10.1016/j.cattod.2004.07.050>.

[31] R. Álvarez, A. Tóffolo, V. Pérez, C.F. Linares, Synthesis and characterization of CoMo/Zn-Al mixed oxide catalysts for hydrosulfurization of thiophene, *Catal. Letters* 137 (2010) 150–155, <https://doi.org/10.1007/s10562-010-0337-9>.

[32] A. Guevara-Lara, A.E. Cruz-Pérez, Z. Contreras-Valdez, J. Mogica-Betancourt, A. Alvarez-Hernández, M. Vrinat, Effect of Ni promoter in the oxide precursors of MoS₂/MgO-Al₂O₃ catalysts tested in dibenzothiophene hydrosulfurization, *Catal. Today* 149 (2010) 288–294, <https://doi.org/10.1016/j.cattod.2009.09.014>.

[33] C. Leyva, M.S. Rana, J. Ancheyta, Surface characterization of Al₂O₃-SiO₂ supported NiMo catalysts: an effect of support composition, *Catal. Today* 130 (2008) 345–353, <https://doi.org/10.1016/j.cattod.2007.10.113>.

[34] G. Li, W. Li, M. Zhang, K. Tao, Morphology and hydrosulfurization activity of CoMo sulfide supported on amorphous ZrO₂ nanoparticles combined with Al₂O₃, *Appl. Catal. A Gen.* 273 (2004) 233–238, <https://doi.org/10.1016/j.apcata.2004.06.038>.

[35] E. Altamirano, J.A. de los Reyes, F. Murrieta, M. Vrinat, Hydrodesulfurization of 4,6-dimethylbenzothiophene over Co(Ni)MoS₂ catalysts supported on alumina: effect of gallium as an additive, *Catal. Today* 133–135 (2008) 292–298, <https://doi.org/10.1016/j.cattod.2007.12.085>.

[36] T. Usman, I. Kubota, Y. Hiromitsu, Okamoto, Effect of boron addition on the surface structure of Co-Mo/Al₂O₃ catalysts, *J. Catal.* 247 (2007) 78–85, <https://doi.org/10.1016/j.jcat.2007.01.010>.

[37] C. Flego, V. Arrigoni, M. Ferrari, R. Riva, L. Zanibelli, Mixed oxides as a support for new CoMo catalysts, *Catal. Today* 65 (2001) 265–270, [https://doi.org/10.1016/S0920-5861\(00\)00560-5](https://doi.org/10.1016/S0920-5861(00)00560-5).

[38] J.M. Herrera, J. Reyes, P. Roquero, T. Klimova, New hydrotreating NiMo catalysts supported on MCM-41 modified with phosphorus, *Microporous Mesoporous Mater.* 83 (2005) 283–291, <https://doi.org/10.1016/j.micromeso.2005.05.010>.

[39] S. Garg, K. Soni, G.M. Kumaran, M. Kumar, J.K. Gupta, L.D. Sharma, G.M. Dhar, Effect of Zr-SBA-15 support on catalytic functionalities of Mo, CoMo, NiMo hydrotreating catalysts, *Catal. Today* 130 (2008) 302–308, <https://doi.org/10.1016/j.cattod.2007.10.082>.

[40] S. Zeng, J. Blanchard, M. Breyses, Y. Shi, X. Su, H. Nie, D. Li, Mesoporous materials from zeolite seeds as supports for nickel-tungsten sulfide active phases: part 2. Catalytic properties for deep hydrosulfurization reactions, *Appl. Catal. A Gen.* 298 (2006) 88–93, <https://doi.org/10.1016/j.apcata.2005.09.026>.

[41] R. Nava, R.A. Ortega, G. Alonso, C. Ornelas, B. Pawelec, J.L.G. Fierro, CoMo/Ti-SBA-15 catalysts for dibenzothiophene desulfurization, *Catal. Today* 127 (2007) 70–84, <https://doi.org/10.1016/j.cattod.2007.02.034>.

[42] L. Kaluza, Activity of transition metal sulfides supported on Al₂O₃, TiO₂ and ZrO₂ in the parallel hydrosulfurization of 1-benzothiophene and hydrogenation of 1-methyl-cyclohex-1-ene, *Reac Kinet Mech Cat* 114 (2015) 781–794, <https://doi.org/10.1007/s11144-014-0809-9>.

[43] M. Li, H. Li, F. Jiang, Y. Chu, H. Nie, The relation between morphology of (Co)MoS₂ phases and selective hydrosulfurization for CoMo catalysts, *Catal. Today* 149 (2010) 35–39, <https://doi.org/10.1016/j.cattod.2009.03.017>.

[44] T. Mochizuki, H. Itou, M. Toba, Y. Miki, Y. Yoshimura, Effects of acidic properties on the catalytic performance of CoMo sulfide catalysts in selective hydrosulfurization of gasoline fractions, *Energy Fuels* V. 22 (2008) 1456–1462.

[45] D.J. Pérez-Martínez, E.M. Gaigneaux, S.A. Giraldo, A. Centeno, Interpretation of the catalytic functionalities of CoMo/ASA FCC-naphtha-HDT catalysts based on its acid properties, *J. Mol. Catal. A Chem.* 335 (2011) 112–120, <https://doi.org/10.1016/j.molcata.2010.11.022>.

[46] D.J. Pérez-Martínez, E.M. Gaigneaux, S.A. Giraldo, Improving the selectivity to HDS in the HDT of synthetic FCC naphtha using sodium doped amorphous aluminosilicates as support of CoMo catalysts, *Appl. Catal. A Gen.* 421–422 (2012) 48–57, <https://doi.org/10.1016/j.apcata.2012.01.036>.

[47] K.A. Nadeina, O.V. Klimov, I.G. Danilova, V.Y. Pereyma, E.Y. Gerasimov, I.P. Prosvirin, A.S. Noskov, Amorphous silica-alumina – perspective supports for selective hydrotreating of FCC gasoline: influence of Mg, *Appl. Catal. B Environ.* 223 (2018) 22–35, <https://doi.org/10.1016/j.apcata.2017.07.004>.

[48] T. Klimova, D. Casados, J. Ramírez, New selective Mo and NiMo HDS catalysts supported on Al₂O₃-MgO(x) mixed oxides, *Catal. Today* 43 (1998) 135–146 <http://www.sciencedirect.com/science/article/pii/S0920586198001424>.

[49] G. Muralidhar, F.E. Massoth, J. Shabtai, Catalytic functionalities of supported sulfides, *J. Catal.* 85 (1984) 44–52, [https://doi.org/10.1016/0021-9517\(84\)90108-8](https://doi.org/10.1016/0021-9517(84)90108-8).

[50] X. Chun-e, C. Yong-ming, L.I.U. Chen-guang, Effect of phosphorus on the hydrosulfurization and hydrodenitrogenation performance of presulfidized NiMo/Al₂O₃ catalyst, *J. Fuel Chem. Technol.* 39 (2011) 355–360, [https://doi.org/10.1016/S1872-5813\(11\)60026-1](https://doi.org/10.1016/S1872-5813(11)60026-1).

[51] Z. Tong-na, Y.I.N. Hai-liang, L.I.U. Yun-qi, H.A.N. Shu-na, C. Yong-ming, L.I.U. Chen-guang, Effect of phosphorus content on the active phase structure of NiMoP/Al₂O₃ catalyst, *J. Fuel Chem. Technol.* 38 (2010), [https://doi.org/10.1016/S1872-5813\(10\)60020-5](https://doi.org/10.1016/S1872-5813(10)60020-5).

[52] S. Sigurdson, V. Sundaramurthy, A.K. Dalai, J. Adjaye, Phosphorus promoted trimetallic NiMoW/γ-Al₂O₃ sulfide catalysts in gas oil hydrotreating, *J. Mol. Catal. A Chem.* 291 (2008) 30–37, <https://doi.org/10.1016/j.molcata.2008.05.011>.

[53] S.K. Maity, G.A. Flores, J. Ancheyta, M.S. Rana, Effect of preparation methods and content of phosphorus on hydrotreating activity, *Catal. Today* 130 (2008) 374–381, <https://doi.org/10.1016/j.cattod.2007.10.100>.

[54] S. Kasztelan, H. Touhoat, J. Grimalt, J.P. Bonnelle, A geometrical model of the active phase of hydrotreating catalysts, *Appl. Catal.* 13 (1984) 127–159, [https://doi.org/10.1016/S0166-9834\(00\)83333-3](https://doi.org/10.1016/S0166-9834(00)83333-3).

[55] A.D. Gandubert, C. Legens, D. Guillaume, S. Rebourg, E. Payen, X-ray photoelectron spectroscopy surface quantification of sulfided CoMoP catalysts – relation between activity and promoted sites – part I: influence of the Co/Mo Ratio, *Oil Gas Sci. Technol. Rev. IFP.* 62 (2007) 79–90.

[56] A.D. Gandubert, E. Krebs, C. Legens, D. Costa, D. Guillaume, P. Raybaud, Optimal promoter edge decoration of CoMoS catalysts: a combined theoretical and experimental study, *Catal. Today* 130 (2008) 149–159, <https://doi.org/10.1016/j.cattod.2007.06.041>.

[57] P.A. Nikulshin, D.I. Ishutenko, A.A. Mozhaev, K.I. Maslakov, A.A. Pimerzin, Effects of composition and morphology of active phase of CoMo/Al₂O₃ catalysts prepared using Co₂Mo₁₀-heteropolyacid and chelating agents on their catalytic properties in HDS and HYD reactions, *J. Catal.* 312 (2014) 152–169, <https://doi.org/10.1016/j.jcat.2014.01.014>.

[58] A.M. De Jong, V.H.J. De Beer, J.A.R. Van Veen, J.W. Niemantsverdriet, Surface science model of a working cobalt-promoted molybdenum sulfide hydro-desulfurization catalyst: characterization and reactivity, *J. Phys. Chem.* 100 (1996) 17722–17724, <https://doi.org/10.1021/jp962207d>.

[59] A. Cordova, P. Blanchard, C. Lancelot, G. Frémy, C. Lamonier, Probing the nature of the active phase of molybdenum-supported catalysts for the direct synthesis of methylmercaptan from syngas and H₂S, *ACS Catal.* 5 (2015) 2966–2981, <https://doi.org/10.1021/cs502031f>.

[60] B. Scheffer, N.J.J. Dekker, P.J. Mangnus, J.A. Mouljin, A temperature-programmed reduction study of sulfidized CoMo/Al₂O₃ hydrodesulfurization catalysts, *J. Catal.* 121 (1990) 31–46, [https://doi.org/10.1016/0021-9517\(90\)90214-5](https://doi.org/10.1016/0021-9517(90)90214-5).

[61] G.B. McGarvey, S. Kasztelan, An investigation of the reduction behavior of MoS₂/Al₂O₃ and the subsequent detection of hydrogen on the surface, *J. Catal.* 148 (1994) 149–156, <https://doi.org/10.1006/jcat.1994.1196>.

[62] C. Arrouvel, M. Breysse, H. Toulhoat, P. Raybaud, A density functional theory comparison of anatase (TiO₂)- and γ-Al₂O₃-supported MoS₂ catalysts, *J. Catal.* 232 (2005) 161–178, <https://doi.org/10.1016/j.jcat.2005.02.018>.

[63] D. Costa, C. Arrouvel, M. Breysse, H. Toulhoat, P. Raybaud, Edge wetting effects of γ-Al₂O₃ and anatase-TiO₂ supports by MoS₂ and CoMoS active phases: a DFT study, *J. Catal.* 246 (2007) 325–343, <https://doi.org/10.1016/j.jcat.2006.12.007>.

[64] E.A. Permyakov, V.S. Dorokhov, V.V. Maximov, P.A. Nikulshin, A.A. Pimerzin, V.M. Kogan, Computational and experimental study of the second metal effect on the structure and properties of bi-metallic MeMoS-sites in transition metal sulfide catalysts, *Catal. Today* 305 (2018) 19–27, <https://doi.org/10.1016/j.cattod.2017.10.041>.

[65] P. Castillo-Villalón, J. Ramírez, R. Cuevas, P. Vázquez, R. Castañeda, Influence of the support on the catalytic performance of Mo, CoMo, and NiMo catalysts supported on Al₂O₃ and TiO₂ during the HDS of thiophene, dibenzothiophene, or 4,6-dimethylbenzothiophene, *Catal. Today* 259 (2016) 140–149, <https://doi.org/10.1016/j.cattod.2015.06.008>.

[66] Y. Ji, P. Afanasiev, M. Vrinat, W. Li, C. Li, Promoting effects in hydrogenation and hydrodesulfurization reactions on the zirconia and titania supported catalysts, *Appl. Catal. A Gen.* 257 (2004) 157–164, <https://doi.org/10.1016/j.apcata.2004.02.039>.

[67] L. Kaluža, D. Gulková, Effect of promotion metals on the activity of MoS₂/ZrO₂ catalyst in the parallel hydrodesulfurization of 1-benzothiophene and hydrogenation of 1-methyl-cyclohex-1-ene, *React. Kinet. Mech. Catal.* 118 (2016) 313–324, <https://doi.org/10.1007/s11144-016-1002-0>.

[68] J. Mazurelle, C. Lamonier, C. Lancelot, E. Payen, C. Pichon, D. Guillaume, Use of the cobalt salt of the heteropolyanion [Co₂Mo₁₀O₃₈H₄]⁶⁻ for the preparation of CoMo HDS catalysts supported on Al₂O₃, TiO₂ and ZrO₂, *Catal. Today* 130 (2008) 41–49, <https://doi.org/10.1016/j.cattod.2007.07.008>.